NOVEL DESIGN OF A PASSIVE MICROFLUIDIC MIXER FOR BIOCHEMICAL REACTIONS AND BIOSENSING

A Thesis

by

YAO-CHUNG YEE

Submitted to the Office of Graduate Studies of
Texas A&M University
in partial fulfillment of the requirements for the degree of

MASTER OF SCIENCE

August 2007

Major Subject: Electrical Engineering

NOVEL DESIGN OF A PASSIVE MICROFLUIDIC MIXER FOR BIOCHEMICAL REACTIONS AND BIOSENSING

A Thesis

by

YAO-CHUNG YEE

Submitted to the Office of Graduate Studies of
Texas A&M University
in partial fulfillment of the requirements for the degree of

MASTER OF SCIENCE

Approved by:

Chair of Committee,	Jun Kameoka
Committee Members,	Chin B. Su
	Peng Li
	Kuang-An Chang
Head of Department,	Costas N. Georghiades

August 2007

Major Subject: Electrical Engineering

ABSTRACT

Novel Design of a Passive Microfluidic Mixer for Biochemical Reactions and Biosensing. (August 2007)

Yao-Chung Yee, B.S., The University of Texas at Austin

Chair of Advisory Committee: Dr. Jun Kameoka

The next step in miniaturization of analytical devices involves the use of MEMS and Lab-on-a-Chip applications, where many biological or chemical reactions are carried out on the device in real time. Since detection mechanisms occur almost immediately after the reactions, inefficient mixing of reagents could cause a decrease in sensing capability, especially on micro- and nano-scaled devices. Thus a microfluidic mixer has become a crucial component in these applications.

Here we propose a new design of a passive microfluidic mixer that utilizes the theories of chaotic advection to enhance mixing. The micro-channels for the mixer have dimensions with width ranging from $10\,\mu m$ to $40\,\mu m$, depth $40\,\mu m$, and a total length of $280\,\mu m$. First the designs are simulated using CFD-ACE+ for computational analysis. After the device geometry has been decided, the actual devices are fabricated using traditional UV photolithography on silicon and bonded with pyrex glass by anodic bonding. To test the actual device mixing efficiency, we used a fluorescent dye rhodamine B solution to mix with DI water and put the devices under fluorescent microscope observations for real-time analysis. Images of fluorescent light intensities

are taken at different flow rates during the analysis and are later used to study the experimental results calculated using a published mixing efficiency formula for comparison.

ACKNOWLEDGMENTS

I would like to thank my advisor Dr. Jun Kameoka for his guidance and support during my research and learning. I would also like to thank my committee members, Dr. Chin Su, Dr. Peng Li, and Dr. Kuang-An Chang for reviewing my thesis and providing me positive suggestions.

In addition, I want to thank Chao-Kai Chou at the M. D. Anderson Cancer Center for providing the necessary samples and equipment for the experiments, and our group member Nan Jing for fabricating the silicon wafer devices from Cornell University.

Finally, I would like to express my gratitude and share my happiness with my parents, whose support and encouragement made all this possible.

NOMENCLATURE

BioMEMS	Biological Micro-Electrical-Mechanical System
μ-TAS	Micro-Total-Analysis System
CFD	Computational Fluidic Dynamics

TABLE OF CONTENTS

Page

ABSTRACT iii

ACKNOWLEDGMENTS v

NOMENCLATURE vi

TABLE OF CONTENTS vii

LIST OF FIGURES ix

LIST OF TABLES xi

1. INTRODUCTION 1

    1.1 Active Mixers 2
    1.2 Passive Mixers 4

2. BACKGROUND 7

    2.1 Mixing Theories 7
    2.2 Design Concept 7
    2.3 Design Parameters 9

3. DESIGN AND SIMULATION 11

    3.1 Design Dimension 11
    3.2 Design Simulation 12

4. FABRICATION 15

Page

5. EXPERIMENTAL 19

5.1 Experimental Setup 19
5.2 Experimental Observation 19

6. EVALUATIONS AND RESULTS 21

7. CONCLUSION 36

REFERENCES 39

VITA 41

LIST OF FIGURES

FIGURE		Page
1	Active mixer designs	3
2	Examples of passive mixers	5
3	Coanda effect	8
4	Whirlpool design diagram	9
5	Whirlpool device design and dimensions	11
6	Concentration plots from CFD-ACE+ at various flow speeds	13
7	Velocity vector plots from CFD-ACE+ at various flow speeds	14
8	Fabrication process	16
9	SEM photo of whirlpool design	17
10	Fabricated wafer containing the mixer devices	18
11	Experimental setup at the Axiophot fluorescent microscope	20
12	Edge to edge (W) and bright area (B) measurement and usage	22
13	Edge-to-edge and bright-area image	23
14	Outlet intensity profile measurement	24
15	Light microscope image of whirlpool design	26

FIGURE Page

16 Whirlpool at low flow rates (1 µL/min ~ 10 µL/min)..... 27

17 Whirlpool at mid flow rates (25 µL/min ~ 75 µL/min) 28

18 Whirlpool at high flow rates (100 µL/min ~ 150 µL/min)..... 29

19 Light microscope image of Y-channel..... 30

20 Y-channel at low flow rates (0.5 µL/min ~ 2.5 µL/min). 31

21 Y-channel at mid flow rates (12.5 µL/min ~ 37.5 µL/min)..... 32

22 Y-channel at high flow rates (50 µL/min ~ 75 µL/min). 33

23 Overall mixing performance chart. 35

24 Immuno-precipitation procedure..... 37

LIST OF TABLES

TABLE Page

1 Mixing percentage for whirlpool and Y-channel at various flow rates 34

2 Mixing performance comparison with other designs 35

1. INTRODUCTION

In recent years there has been an increasing interest in the design of microfluidic devices. The miniaturization of fluidic systems provides new applications in biochemical and biomedical fields previously unable to achieve. Entire laboratories can be integrated on a single chip that is portable and disposable. Some of the examples include inkjet printing technique used on DNA and cell printing[1], characterization and separation of reagents due to difference in kinetic and diffusion constants[2], electrophoresis for DNA sequencing on chip[3], and cell arrays for pharmaceutical testing[4]. There are many reasons for using a microfluidic device compared to the traditional methods:

- To combine multiple functions onto one device, and be capable for mass production.
- To manipulate a large amount biological or chemical reactions simultaneously.
- To detect single molecules in narrow channels with laser excitation or fluorescence at low sample concentration.
- Good surface-to-volume ratio enables fast heat and mass transfer as well as chemical bonding process.
- The advances in device fabrication in micro- and nano- scale make the production process quick and inexpensive, thus enable the possibility of multiple-device integration[5].
- The possibility to deploy real-time point-of-care diagnostic tools and drug delivery systems.

This thesis follows the style of *Lab on a Chip.*

Since the ultimate goal of most BioMEMS is to trigger detections at the end, a crucial component of any fluidic system is a mixer to effectively perform the mixing of biological or chemical reagents, so that adequate sensing capability is achieved. However, at the micro- or nano-meter scale, it has traditionally been difficult due to the fact that fluid channels at that dimension has low Reynolds number (Re), an indicator of the fluid turbulence for efficient mixing, and that mixing has mostly been left to molecular diffusion, or laminar flow, which is a very slow process. Only a high value in Re above a critical value (2300 on the macroscale) indicates turbulent flow[4].

1.1 Active Mixers

In order to produce disturbance inside the micro-channels, many mixer designs opt to use active power source to promote mixing. Some examples include utilizing thermal pumps[6] (Figure 1A), electrokinetic force[7], ultrasonic disturbance[8] (Figure 1B), magnetically-driven stirrer[9] (Figure 1C), and optically-driven stirrer[10]. These active mixer designs, although show good results, require an external power source and can be expensive to setup and maintain outside the laboratory environment. Also, moving mechanical parts are prone to wear and tear, and can cause breakage over time. Another equally important issue is bio-compatibility, as extreme heat or laser excitation can kill live cells, rendering the devices ineffective in biological studies.

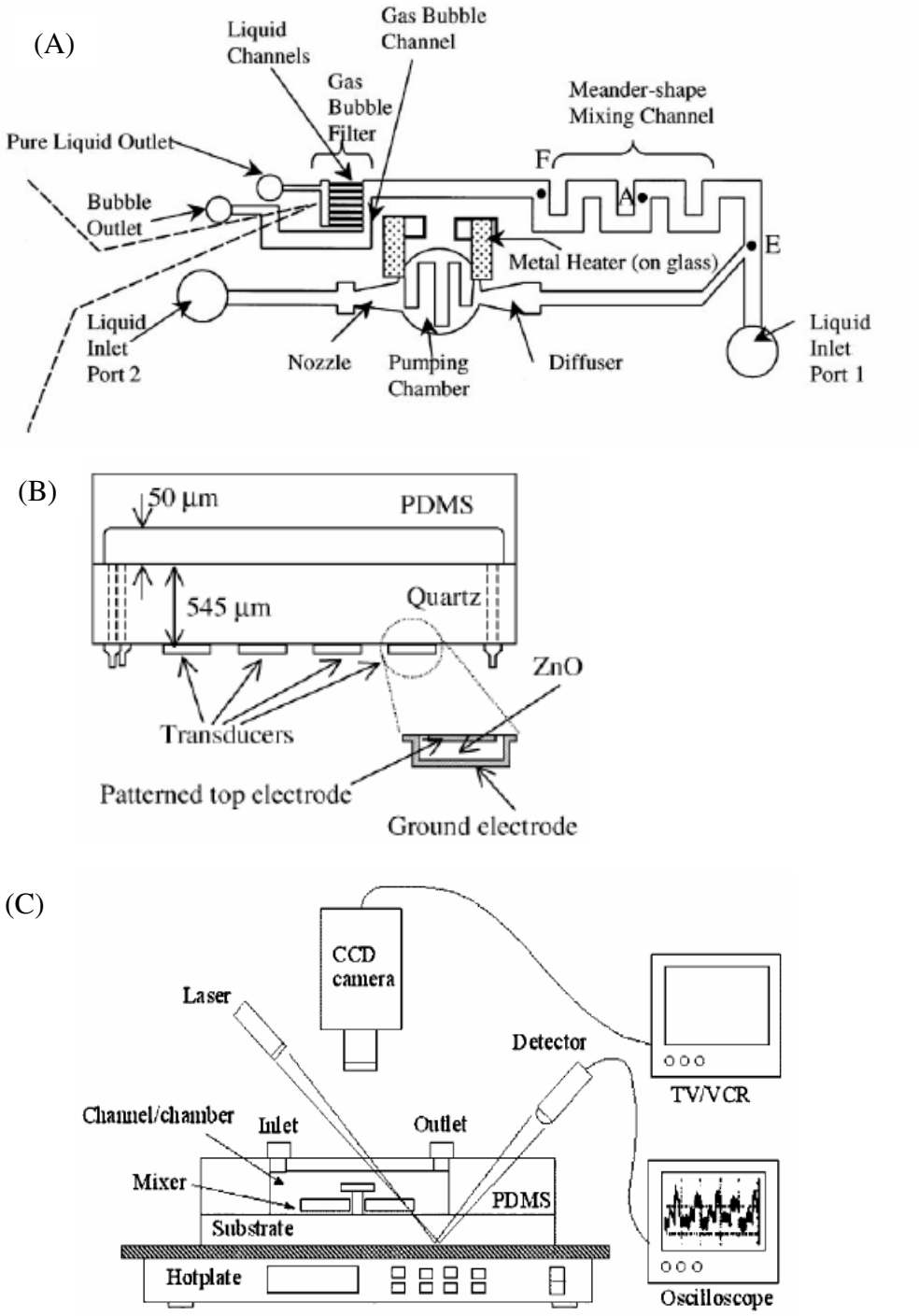

Figure 1. Active mixer designs. (A) Thermal gas-bubble pump mixer[6]; (B) ultrasonic mixer[8]; (C) magnetically-driven stirrer mixer[9].

1.2 Passive Mixers

An alternative to these active mixers are the passive mixers, where mixing is achieved through geometric manipulation of the channels and no external power influence is required. Initial designs started trying to resort to the splitting-merging scheme, shown in Figure 2A, where the mixing stream is split up into multiple sub-streams and then re-merged, to increase the surface contact area for passive diffusion by creating a multi-layer mixing stream, either through 2D or 3D structures[11]. Other designs that are published include mixing by droplets where orientation changes with chaotic advection[12] (Figure 2B), bas-relief structures on the channel floor that disturb the flow pattern[13] (Figure 2C), a self-circulation design that not only attempts to trap mixing fluids in a chamber, but also increases the contact surface of the two mixing reagents[14] (Figure 2D), and a Tesla-structure mixer design that also uses chaotic advection to achieve mixing[15]. Traditionally the passive mixers are under-performing compared to their active counterparts, but they are gaining strength and some recent design can perform equally or better than active mixers. However, some these designs are either only functional at lower flow rates (in the case of a zigzag mixer), very high (in the case of self-circulation), complicated fabrication procedure, or their 3D designs make their integration into a full system unfeasible.

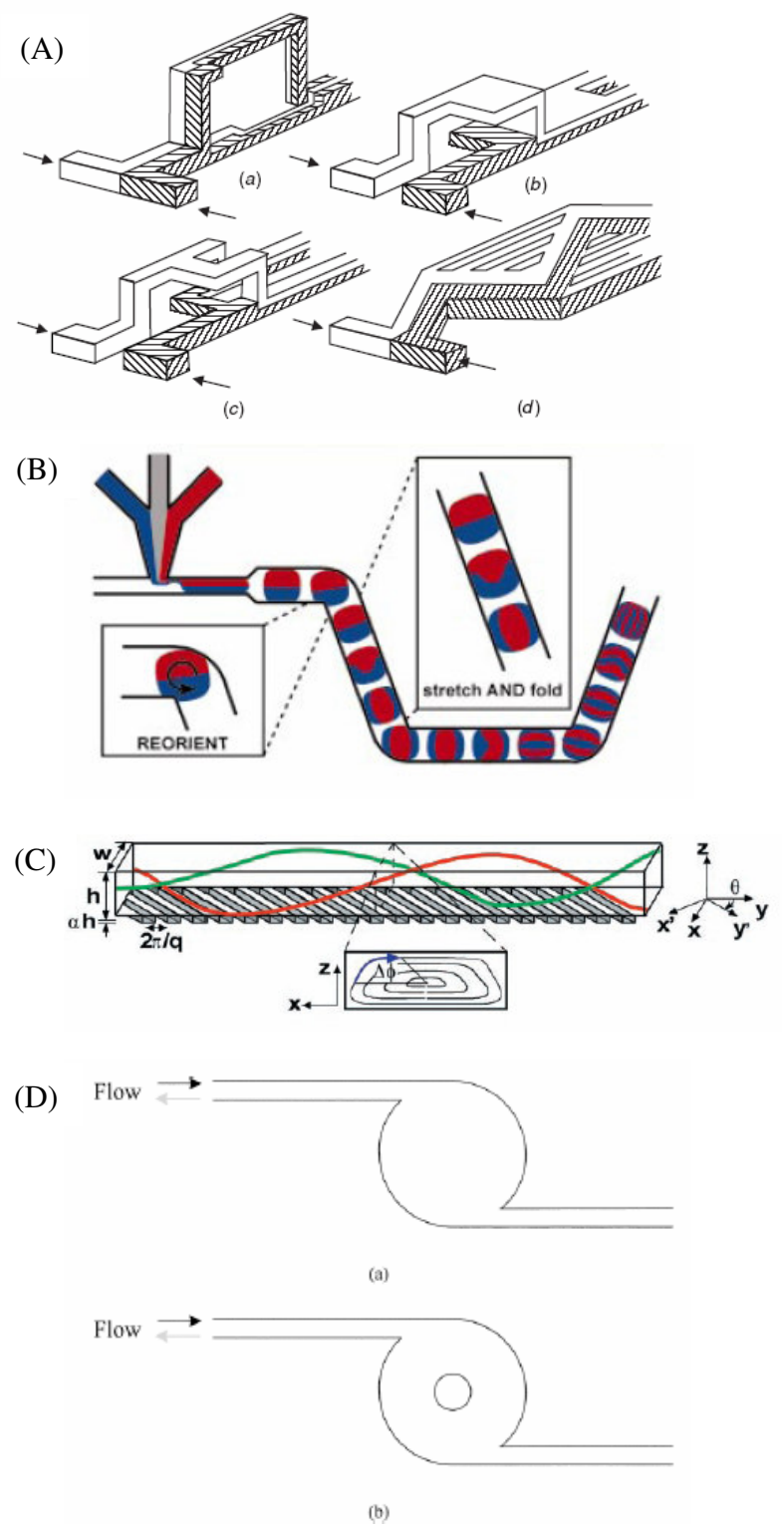

Figure 2. Examples of passive mixers. (A) split-and-join mixers[11]; (B) droplet mixing[12]; (C) bas-relief floor structure mixer[13]; (D) self-circulating mixer[14].

Here we propose a new design that enhances mixing by utilizing chaotic advection, similar to the self-circulation and tesla designs. However our design also uses the split-and-merge scheme, and is more squared-shaped thus dispersions would occur around the corners. The design is an in-plane passive micro-mixer, thus it would have all the benefits of passive mixers, and be easily integrated into a BioMEM or micro total analysis system (μ-TAS).

2. BACKGROUND

2.1 Mixing Theories

As mentioned, typical microfluidic channels have laminar flows, where the mixing is dependent only on passive diffusion, and thus the diffusion coefficient and viscosity of the mixing materials. For simple molecules in aqueous solution, average time to diffuse over distance L is approximately

$$T_D = \frac{L^2}{D}$$

where D is around the order of (10^{-5} cm^2 s^{-1}) [8]. Thus either a very slow flow rate or a very long channel is needed to increase the liquid resident time to achieve mixing. Typical mixing mechanism in a macro-scale mixer is often by turbulence, which is difficult in micro-channels. Turbulences can be generated via external powers, such as a mechanical stirrer inside the channels. However, as mentioned previously, most of these active mixer designs have a complicated setup and expensive maintenance. Another way to enhance mixing in a mixer is by chaotic advection, created by changing the channel geometry and thus a perturbation can occur from the lateral oscillations of the roll patterns where some particles are trapped in a vortex[16]. And at the same time, chaotic advection results in the stretching and folding of the fluid surfaces that enhances mixing. Also, shear dispersions result from vertical shear of horizontal velocity and vertical mixing, thus by creating a large velocity difference between adjacent streams, can also be achieved in a micro-channel.

2.2 Design Concept

In our micro-mixer design, codenamed “whirlpool”, we created a split where shear dispersion would distort the stream. Near the outlet where the two streams merge, we shaped the merging geometry so that a large contact surface is created for impact and diffusion. Through Coanda Effect[17] (see Figure 3) we also expect to see chaotic advection to take place. Serpentine bendings at each turning corner can also enhance mixing as the stream is perturbed, as illustrated in Figure 4.

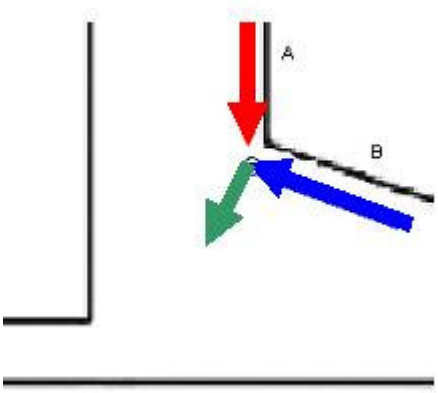

Figure 3. Coanda effect. The blue stream would travel along the wall B, and the red stream would travel along wall A. When contact occurs, there would be dispersion and the mixed green stream would travel towards the outlet.

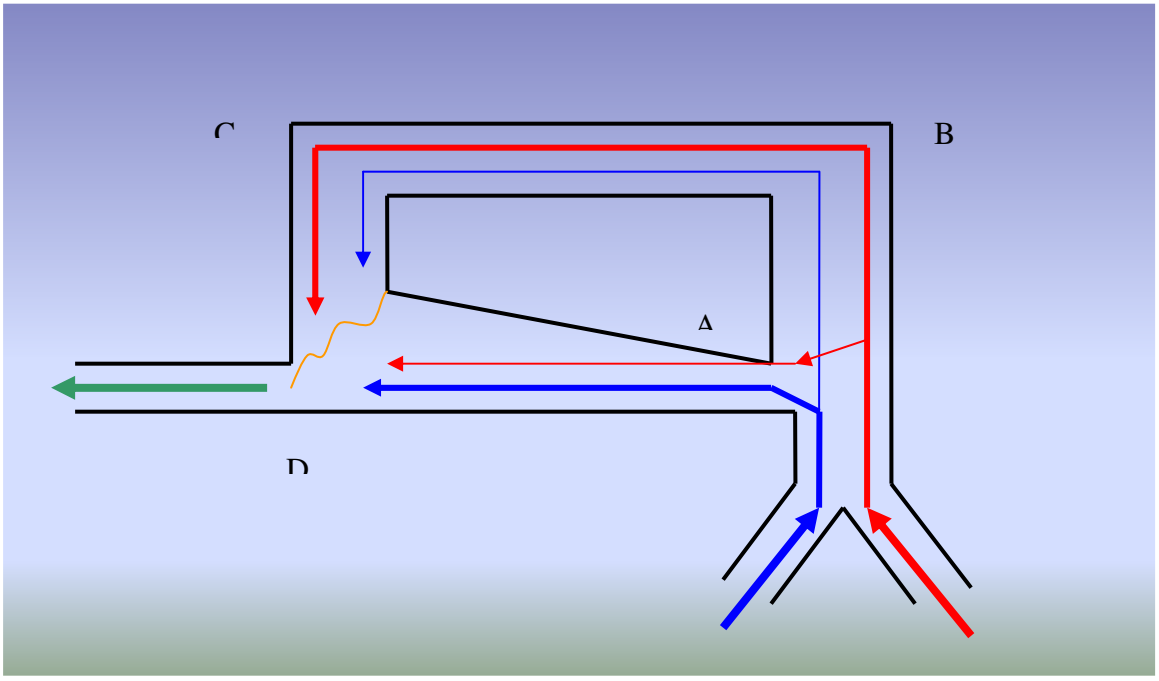

Figure 4. Whirlpool design diagram. (A) When two streams first merge, due to the unique geometry and branching, stretching, folding, and shear dispersion occur; (B) (C) serpentine bendings help enhance mixing as the stream is forced to turn; (D) when two sub-streams re-merge, chaotic advection occurs due to Coanda Effect, and the long contact surface increases diffusion.

2.3 Design Parameters

The conditions inside a micro-channel can be evaluated according to several operating parameters. The most important parameter is the Reynolds number (Re). The Re number provides a value criterion in fluid dynamics that determines the dynamic similitude, where two devices with different fluids and flow rates can have similar fluid flow conditions. Simply put, the Reynolds number serves as an indicator as to how turbulent the fluid flow is. The Reynolds number can be expressed as

$$R_e = \frac{\rho v D_h}{\mu}$$

where ρ is the fluid density, v is the flow velocity, μ is the fluid viscosity, and D_h is the characteristic dimension length[8]. For a rectangular channel, as in our case, the length can be expressed as

$$D_h = \frac{2ab}{a+b}$$

where a and b are dimensions of the channel cross section. Typical Re number in macro-scale devices could range in the hundreds or thousands, while in micro-meter scale low numbers close to single digits are expected in laminar flow conditions. Thus, creating mixers that increase the Reynolds number in micro-scale is often a big consideration in the design. Since fluid viscosity is fixed, increasing the liquid flow velocity and creating channel bending are some ways to increase the Re number. The Re number of up to 500 where flow velocity is as high as 7.60 m s-1 has been reported in micro-channels[18]. However, due to required high driving pressure, relying on flow velocity alone can be difficult on the bonding and interconnect process of the devices, and leakage problems will have to be overcome.

3. DESIGN AND SIMULATION

3.1 Design Dimension

In our "whirlpool" micro-mixer, the incoming laminar stream is split up to a main stream and a sub stream. Due to the angle of the branch (90°), the stream will experience severe stretching and folding in the area, especially at higher flow velocities since the side stream will need to make a bigger turn. And near the exit of the micro-mixer, two streams are rejoined at another 90° angle, thus utilizing the effect of reverse chaotic advection to enhance the mixing. Figure 5 shows the overall design.

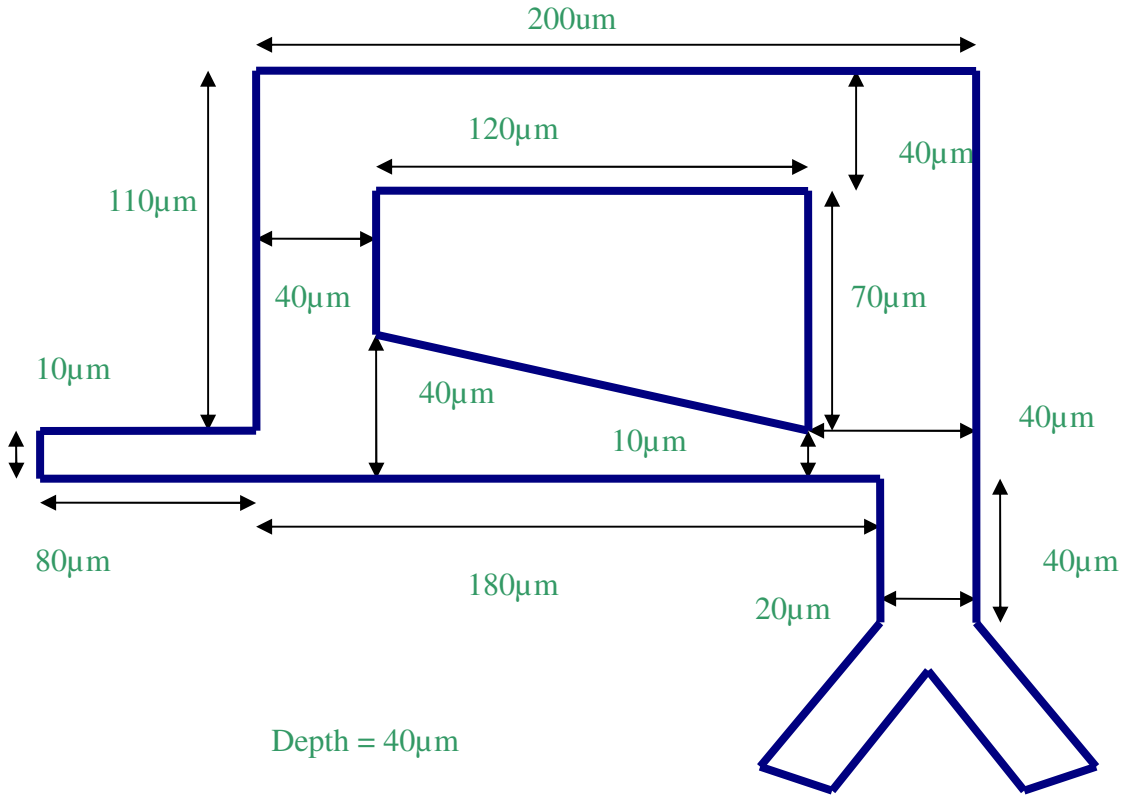

Figure 5. Whirlpool device design and dimensions.

3.2 Design simulation

To investigate the effect of the mixer designs, CFD-ACE+ simulation software from the ESI Group (www.esi-group.com) has been used to analyze the computational results, including concentration and velocity distributions. In the simulations, one of the inlets has DI water, with density = 998.2 kg/m3, viscosity = 0.001003 kg/m-s, and molecular weight = 18.0152 g/mol. The other inlet has an estimated 99% mass fraction of DI water, and 1% mass fraction of Rhodamine B. Rhodamine B serves as the fluorescent dye and has the empirical formula of $C_{28}H_{31}N_2O_3Cl$, with a molecular weight of 479 g/mol, and maximum absorption spectrum around 550 nm. Temperature is set to room temperature (300 K), with standard gravity = 9.98 m2/s, and atmospheric pressure (101325 Pa). And 3D steady mixture models are chosen to provide accuracy, with calculation of concentration. Mixer geometry is generated using CFD-GEOM, and has mesh grids with smallest size of 2μm. The simulations are iterated until the convergence criteria are met, with number of iterations at 300, convergence critical 1e-12, and minimum residual 1e-18. Inlet velocities are set at 0.05 m/s, 1 m/s, and 5 m/s for slow, medium, and high flow velocity simulations, corresponding to roughly 1 μL/min, 20 μL/min, and 100 μL/min, given that the actual device micro-channel has an inlet of 20 μm width x 20 μm depth. According to the simulations, good mixing can be achieved with at the outlet (approximately 470 μm traveling distance from inlet) at the tested flow velocities. The velocity plots also mostly follow our initial estimate, where the vector plots confirming the stretching/folding/dispersion near the split, and the merging near the outlet. The simulation plots are shown in Figure 6 and Figure 7.

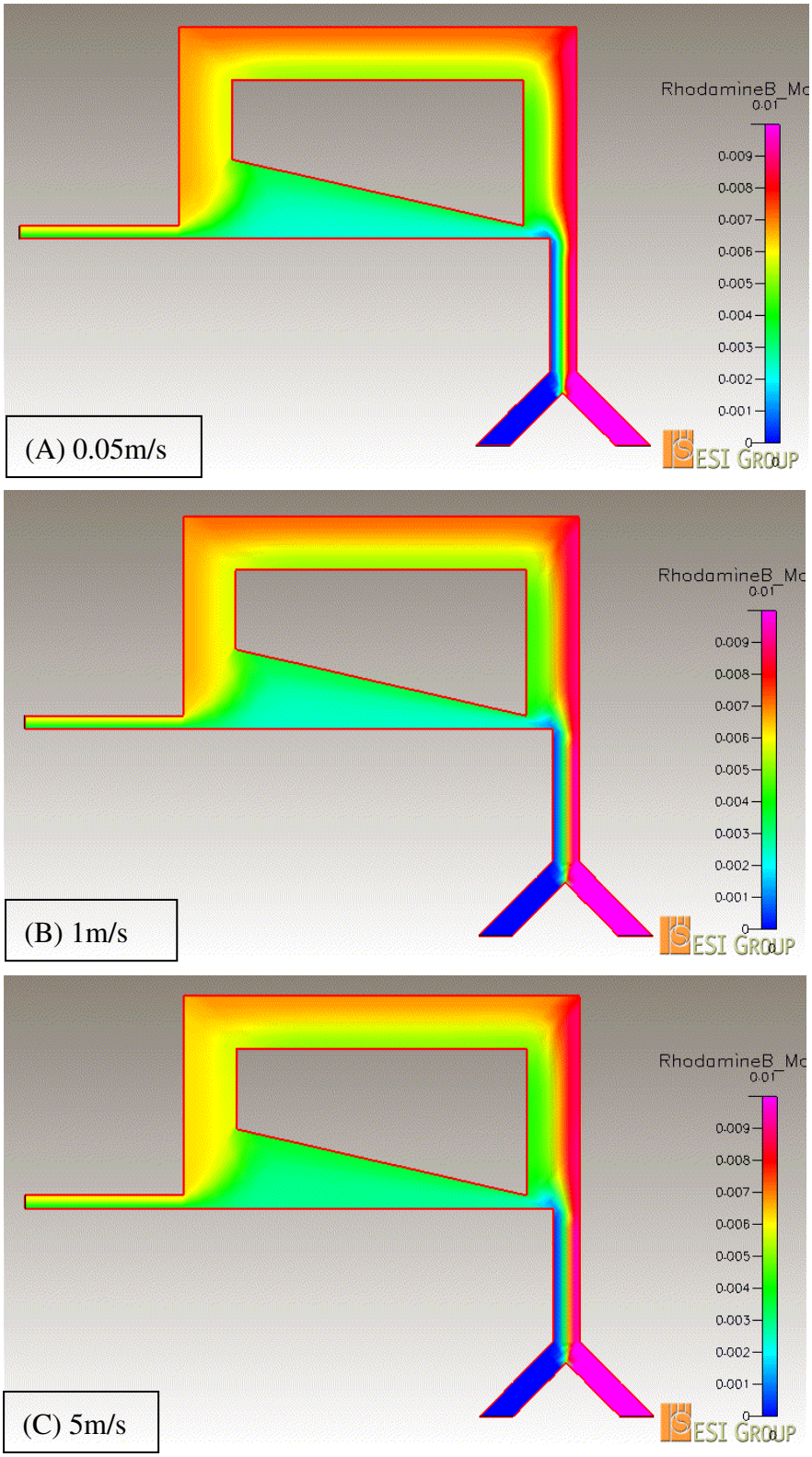

Figure 6. Concentration plots from CFD-ACE+ at various flow speeds.

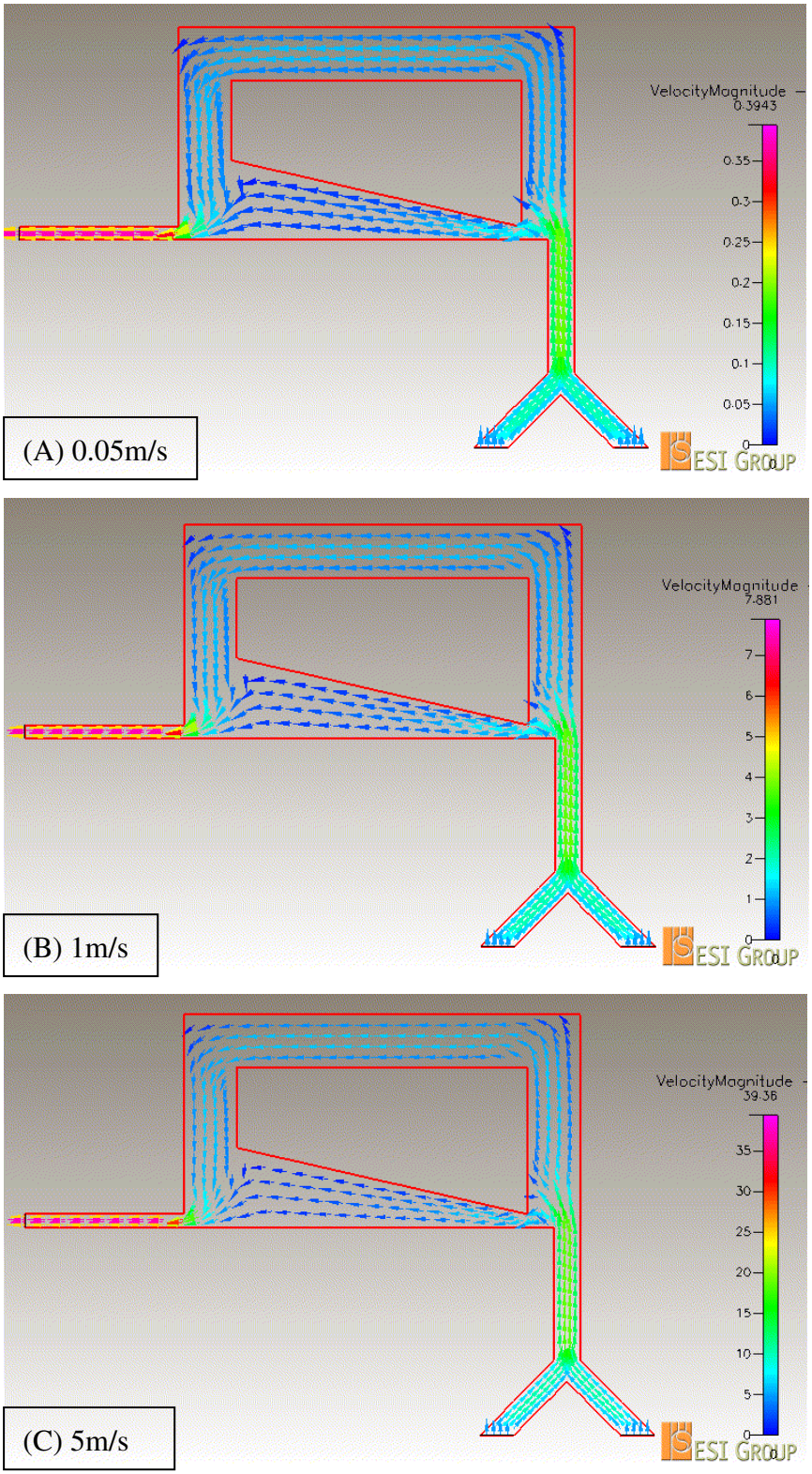

Figure 7. Velocity vector plots from CFD-ACE+ at various flow speeds.

4. FABRICATION

A 4” single crystal silicon wafer, single side polished and 500 um thick, is used as the base wafer. Figure 8 shows the summary of the fabrication steps. The procedure of fabrication is described here.

1. Spin coat P-20 primer (adhesive) and S1813 (photoresist, 1.3um at 4000 rpm, with ramp 2000 rpm/sec) for 30 secondss.
2. Softbake on a hotplate at 115 °C for 1 min.
3. Pattern (UV mask exposure), EV 620 (contact mask aligner) exposure for 4 seconds.
4. MIF 300 (developer after exposure, remove photoresist) develop for 1min.
5. Hardbake on a hotplate at 115 ºC for 1 min.
6. Descum (O2 plasma) in Branson Barrel Etcher for 4 minutes (room temperature).
7. Unaxis 7700 Trench recipe (Bosch process, anisotropic deep etcher on Si) for 30 loops (20 μm).
8. Remove PR using 30mins in resist strip bath and follow with 5 mins Branson Barrel Etcher PR stripe.
9. Spin coat P-20 and FSC-M at 3000 rpm (ramp 1000 rpm/sec) for 1 minute.
10. Air oven bake at 90 °C for 30 minutes.
11. Sand blaster drill thru holes (~1.5mm diameter).
12. Resist strip hot bath for 30 minutes, remove FSC-M.
13. thermal oxidation at 1100 ºC for 30 minutes to 100 nm oxide.
14. Clean sample using hot piranha (3:1 H_2SO_4:H_2O_2).
15. EV 501 anodic bonder with Pyrex glass at 350 °C 1000V for 10 minutes.

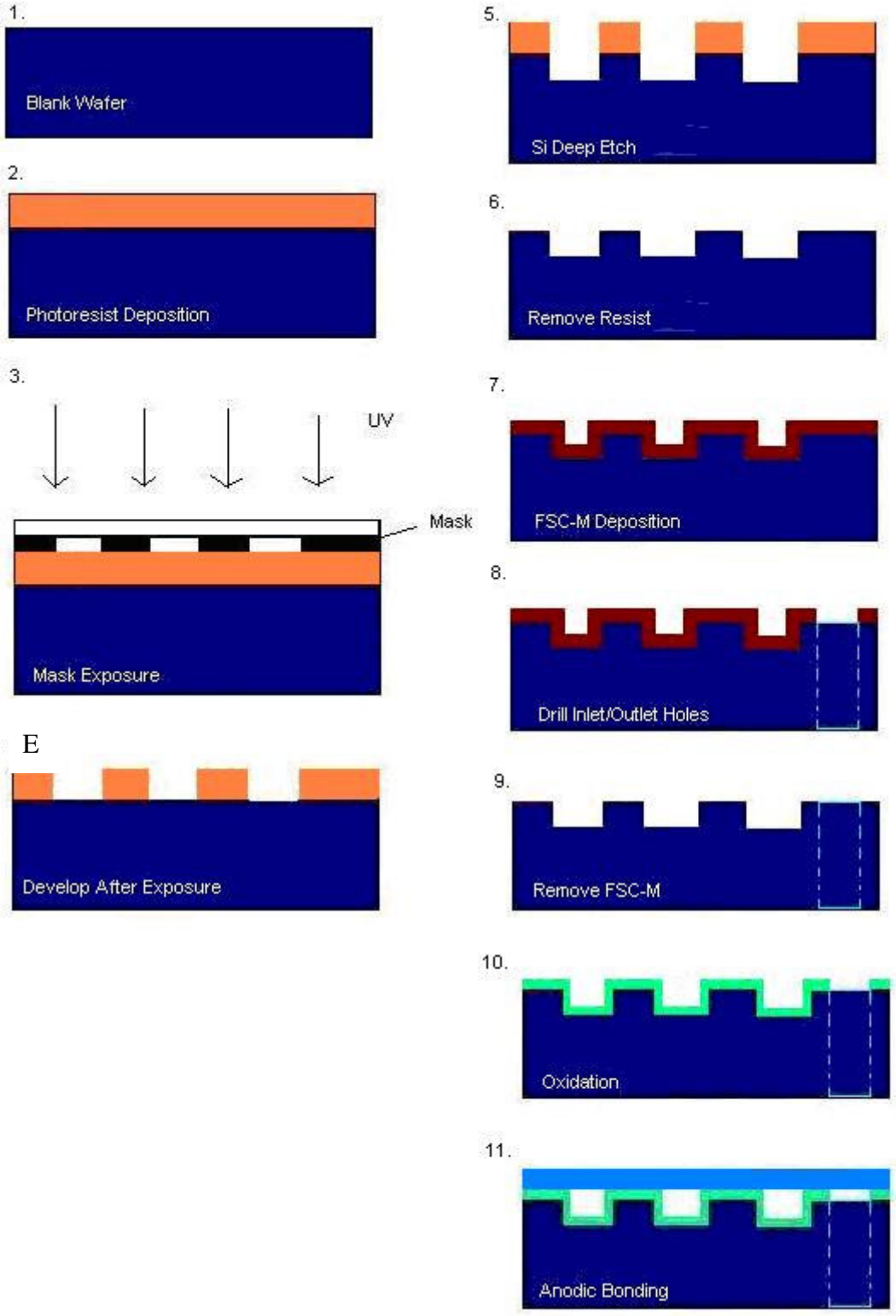

Figure 8. Fabrication process.

Figure 9 shows the SEM image of the fabricated device, and Figure 10 shows the wafer containing the devices.

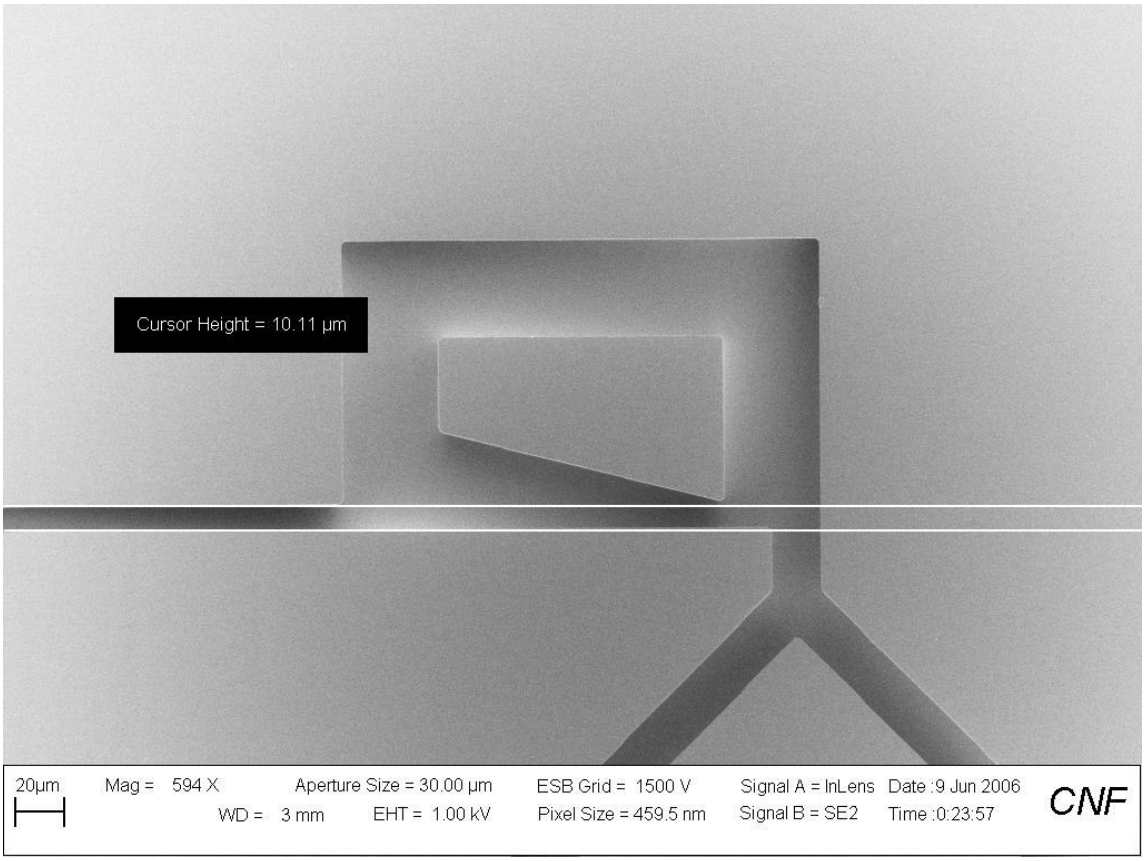

Figure 9. SEM photo of whirlpool design.

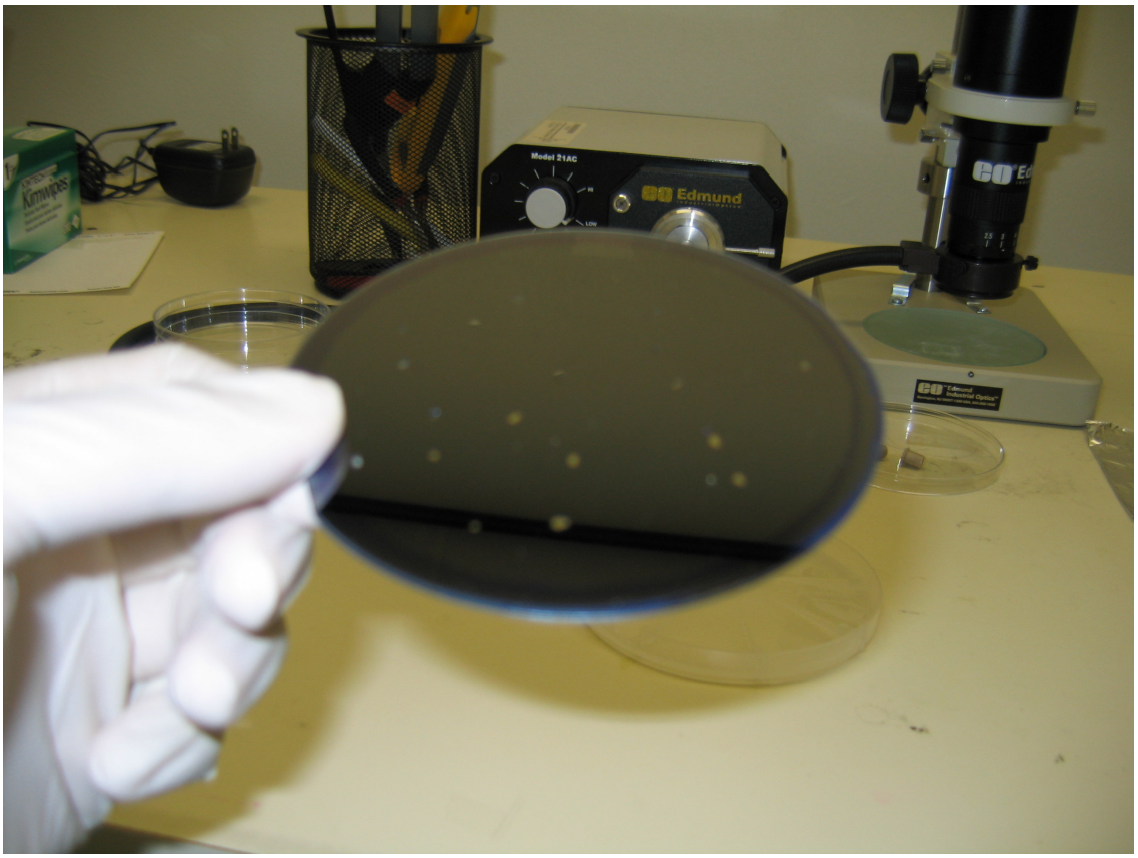

Figure 10. Fabricated wafer containing the mixer devices.

5. EXPERIMENTAL

5.1 Experimental Setup

To analyze the micro-mixer performance in the laboratory, we used Rhodamine B-dyed water with regular DI water for mixture evaluation. The Rhodamine B-dyed water is kept at a concentration of about 0.15 mili-molars. The experiment is carried out under the Zeiss Axiophot fluorescent microscope equipped with CCD cameras while the liquids are being supplied by two syringe pumps by Harvard Apparatus (http://www.instechlabs.com/Pumps/syringe/). Standard 10mL syringe are used to inject the liquids, which are transported through the nanoport tubes from Upchurch Scientific (http://www.upchurch.com) to the devices on the wafer. Fused silica gaskets are applied with epoxy glue to seal with the silicon surface and post-bake in the oven at 75 ℃ for 1 hour. To acquire a quantitative analysis, the imaging software MetaView is used to capture fluorescent images of the mixer device during the experiment, and then analyzed using ImageJ for fluorescent light intensity. The experimental setup is shown in Figure 11.

5.2 Experimental Observation

Two devices are studied under the microscope; the “whirlpool” design and a Y-channel only for comparison. Flow rates of the liquids used on the experiment with the “whirlpool” design ranges from 1 μL/min to 150 μL/min. Because the Y-channel-only device is fabricated with a 20 μm depth, compared to 40 μm of the “whirlpool” design, to provide an equivalent flow velocity, the flow rates of the the Y-channel design is reduced by ½, from 0.5 μL/min to 75 μL/min. First normal light microscope images

are observed to place the device-under-observation in the view center, then UV is applied on the device through the appropriate filters, and reflected light is connected through the microscope objectives and observed on the computer screen. Images are taken through the CCD camera attached on top of the microscope after fluorescent intensity has stabilized in the mixer, and afterwards the mixer is flushed with clean DI water from both inlets before a different flow rate is applied.

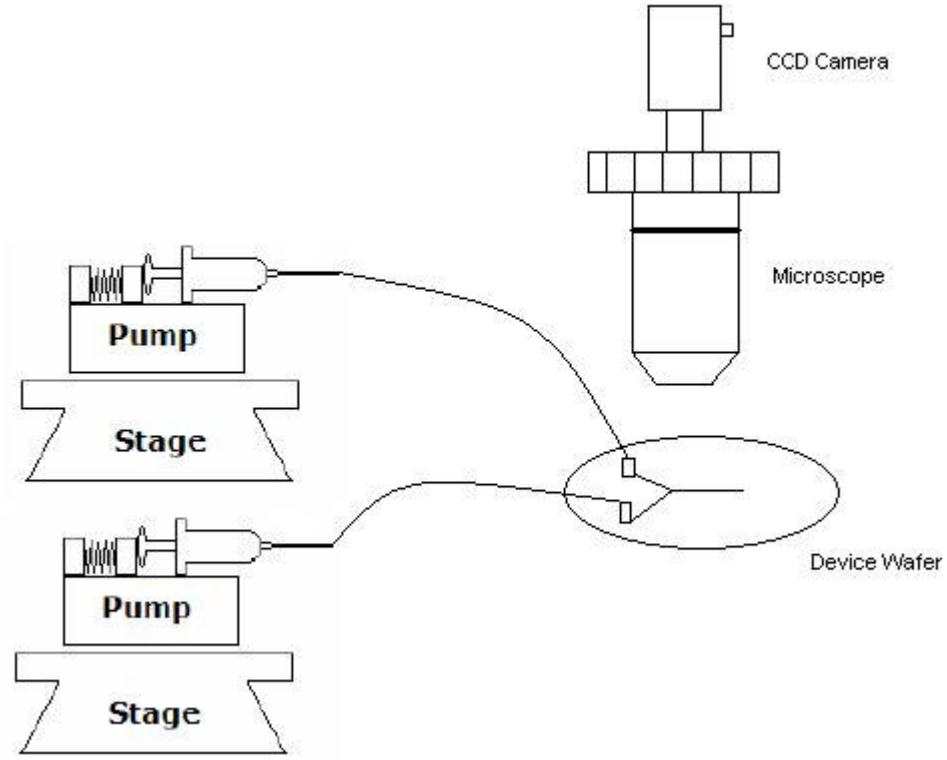

Figure 11. Experimental setup at the Axiophot fluorescent microscope.

6. EVALUATIONS AND RESULTS

The images are analyzed using the software ImageJ™ from the National Institute of Health (http://rsb.info.nih.gov/ij/). First of all, some terms are defined here:

$I_{perfect}$: The theoretical light intensity value for perfectly mixed fluid

$I_{(0)}$: The light intensity value for background (no fluorescence)

I_{max}: The light intensity value for full fluorescent strength

The method of measuring intensity values from the fluorescent images are described as follows:

1. On the light microscope image, channel width from edge to edge (total) and width in the "bright" area (measuring) are measured. Edge to edge distance starts when the "edge drop" in intensity reaches the background intensity value. Bright area width is measured on the plateau in the center, used for $I_{perfect}$ and $I_{(0)}$ flat level width. The values are reserved for inlet and outlet separately, since the channel widths are different. A demonstration is shown in Figure 12.

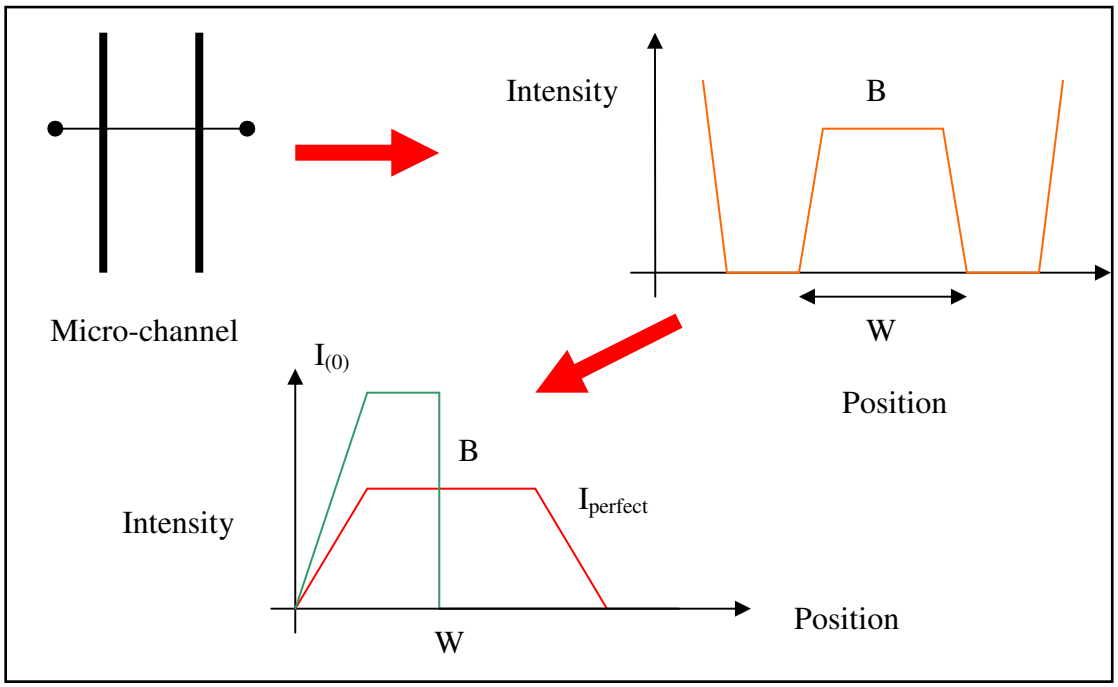

Figure 12. Edge to edge (W) and bright area (B) measurement and usage.

2. On the fluorescent images, n the inlet with Rhodamine B input, a measurement window with width = total inlet width is used to measure maximum intensity value, which is used for normalization, and the edge intensity value, used to identify the edge on the outlet. The maximum intensity value is simply the highest value taken in the measurement window, and the edge intensity value is whatever the values are at the edge distance. The window is shifted until both edge values agree within proximity. The measurement window is 80 µm from the outlet for "whirlpool", and 280 µm downstream for the Y-channel-only. An example of measurement is shown in Figure 13.

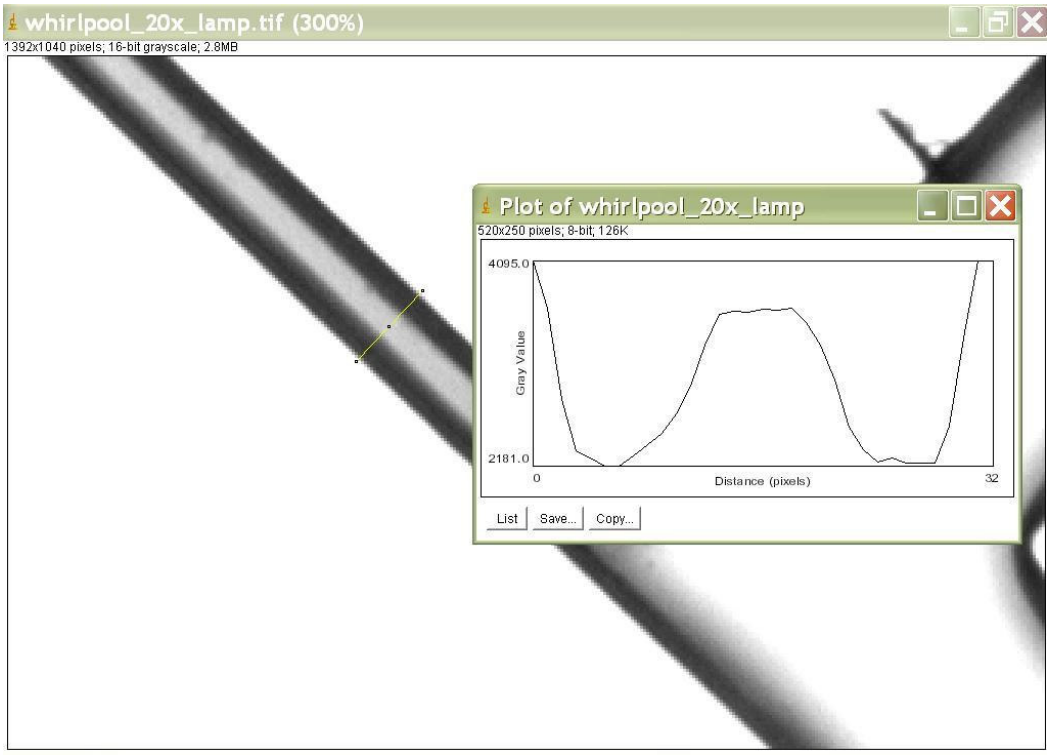

Figure 13. Edge-to-edge and bright-area measurement.

3. Again on the fluorescent images, now on the outlet, again a measurement window with width = total outlet width is used to measure intensity profiles. The measure window is a rectangle, with length twice the size of width, to provide a more accurate average profile. For example, in the Y-channel measurement, the window is 136x68 pixels, thus each of the 68 points in the profile plot is the average of 136 line-width values. Figure 14 shows an example of the measurement.

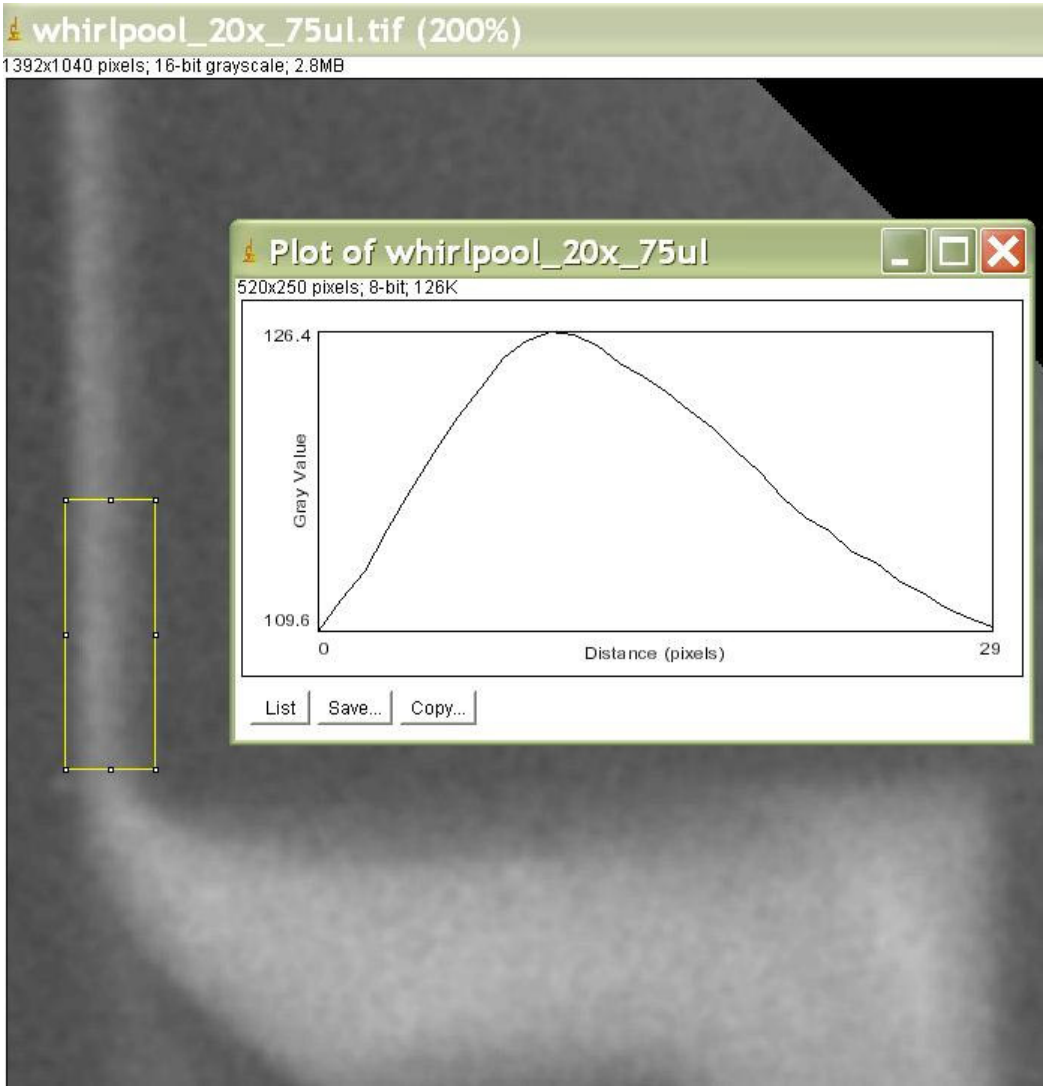

Figure 14. Outlet intensity profile measurement.

To calculate the mixing performances of the devices numerically, we used the formula provided in an article published from the National Institute of Standards and Technology[11], which is as follows:

$$\text{Percentage mixed} = \left(1 - \frac{\sqrt{\frac{1}{N}\sum_{i=1}^{N}\left(I_i - I_i^{Perf}\right)^2}}{\sqrt{\frac{1}{N}\sum_{i=1}^{N}\left(I_i^{0} - I_i^{Perf}\right)^2}} \right) x100$$

where N, I_i, I_i^0, and I_i^{Perf} are the total number of pixels, the intensity at pixel i, the intensity at pixel i if no mixing or diffusion were to occur, and the intensity of the perfectly mixed solution at pixel i, respectively. To use the formula for mixing percentage calculation, $I_{(0)}$, and $I_{perfect}$ profile curves are created. The $I_{perfect}$ profile is linearized to level off at 50% between the maximum intensity value and the background intensity in a normalized plot. $I_{(0)}$ profile is constructed similar to that of $I_{perfect}$, except that the intensity drops off from maximum to minimum in the middle of the channel; thus edge effect is only used on the brighter edge. The $I_{perfect}$ profile identifies that of perfect mixing, which includes rising intensity edge effect on both edges, and flat in the middle, with width equals the "bright" area measured from light microscope images. All images have been smooth-processed to provide a more accurate profile before taking measurements. The results are calculated and plotted using standard spreadsheet application. Figure 15 shows the light microscope image, and Figure 16, 17, 18 show the low, medium, and high velocity fluorescent images for the whirlpool design. Figure 19, 20, 21, 22 show equivalent images for the Y-channel

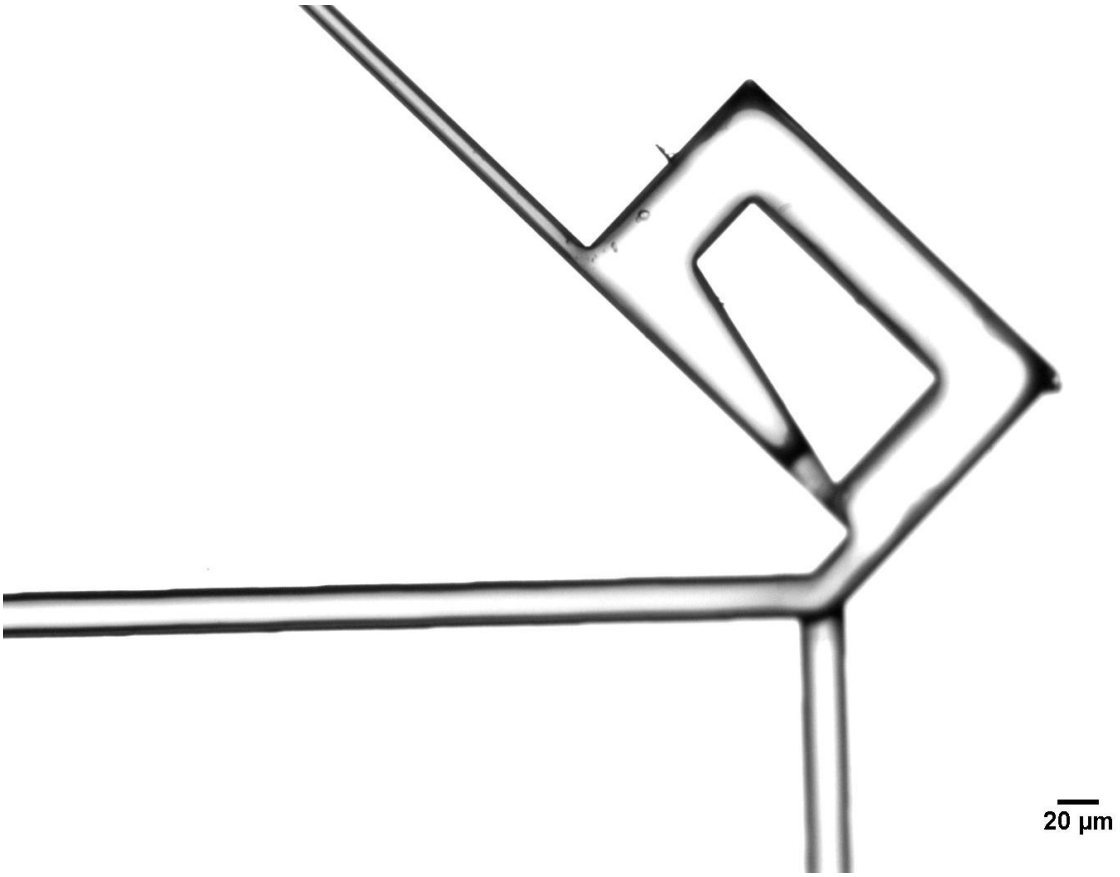

Figure 15. Light microscope image of whirlpool design.

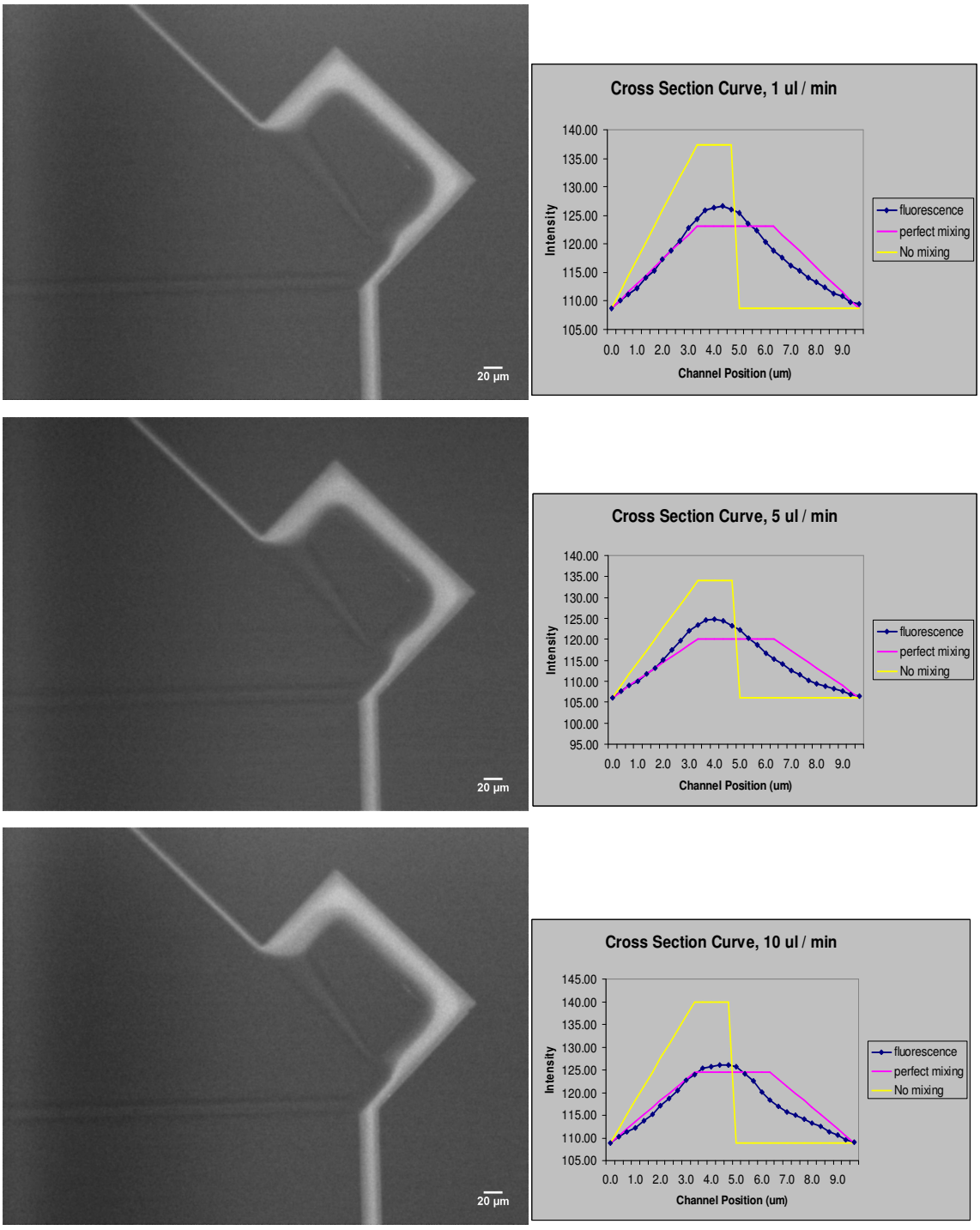

Figure 16. Whirlpool at low flow rates (1 µL/min ~ 10 µL/min).

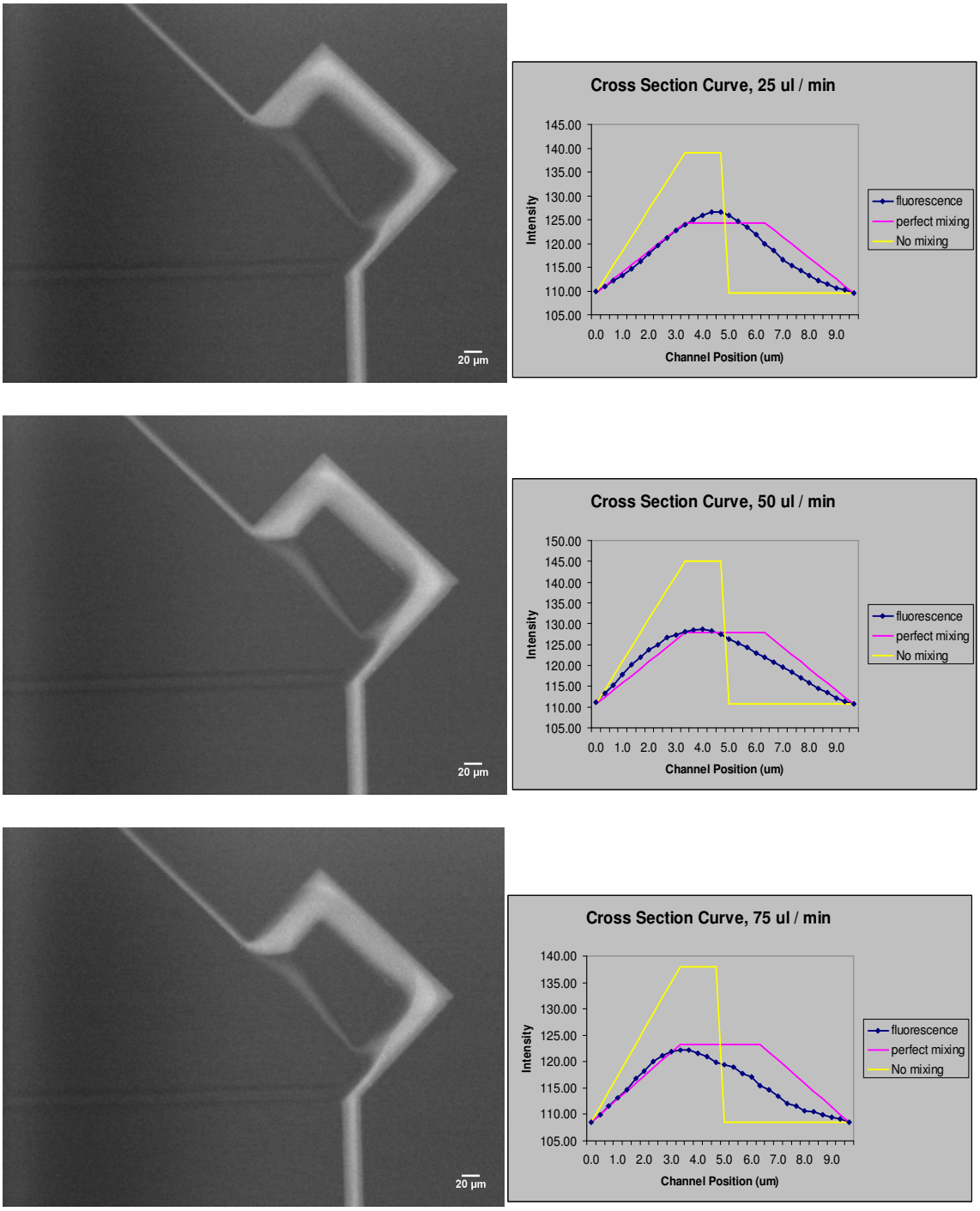

Figure 17. Whirlpool at mid flow rates (25 µL/min ~ 75 µL/min).

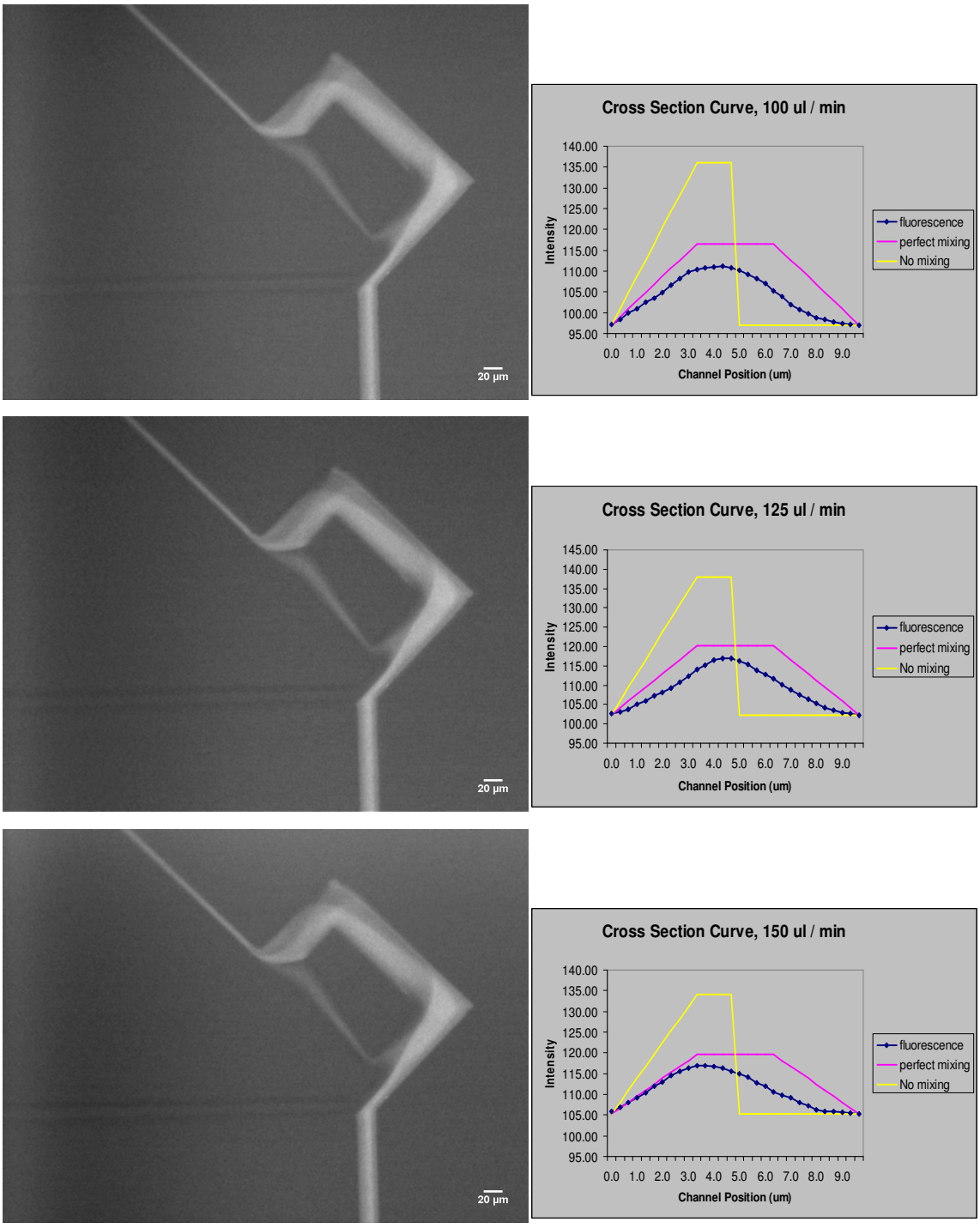

Figure 18. Whirlpool at high flow rates (100 µL/min ~ 150 µL/min).

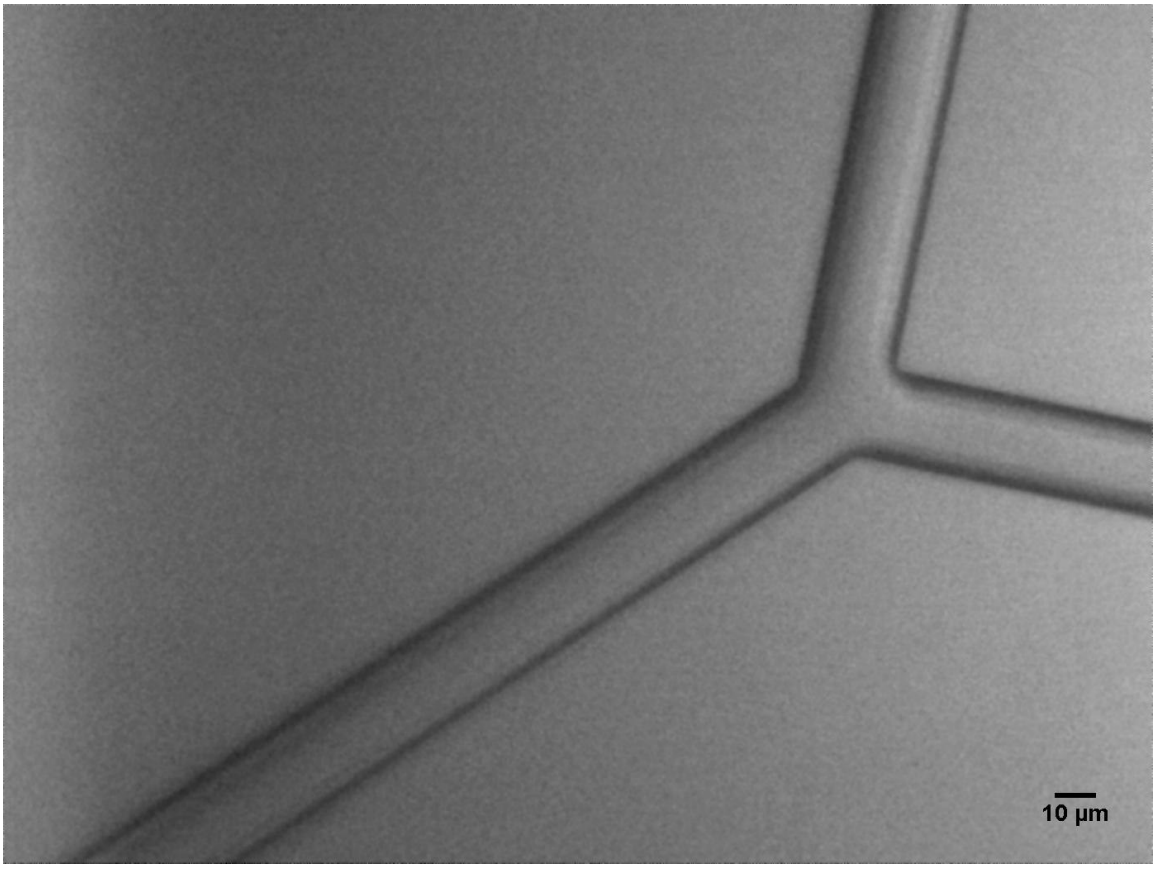

Figure 19. Light microscope image of Y-channel.

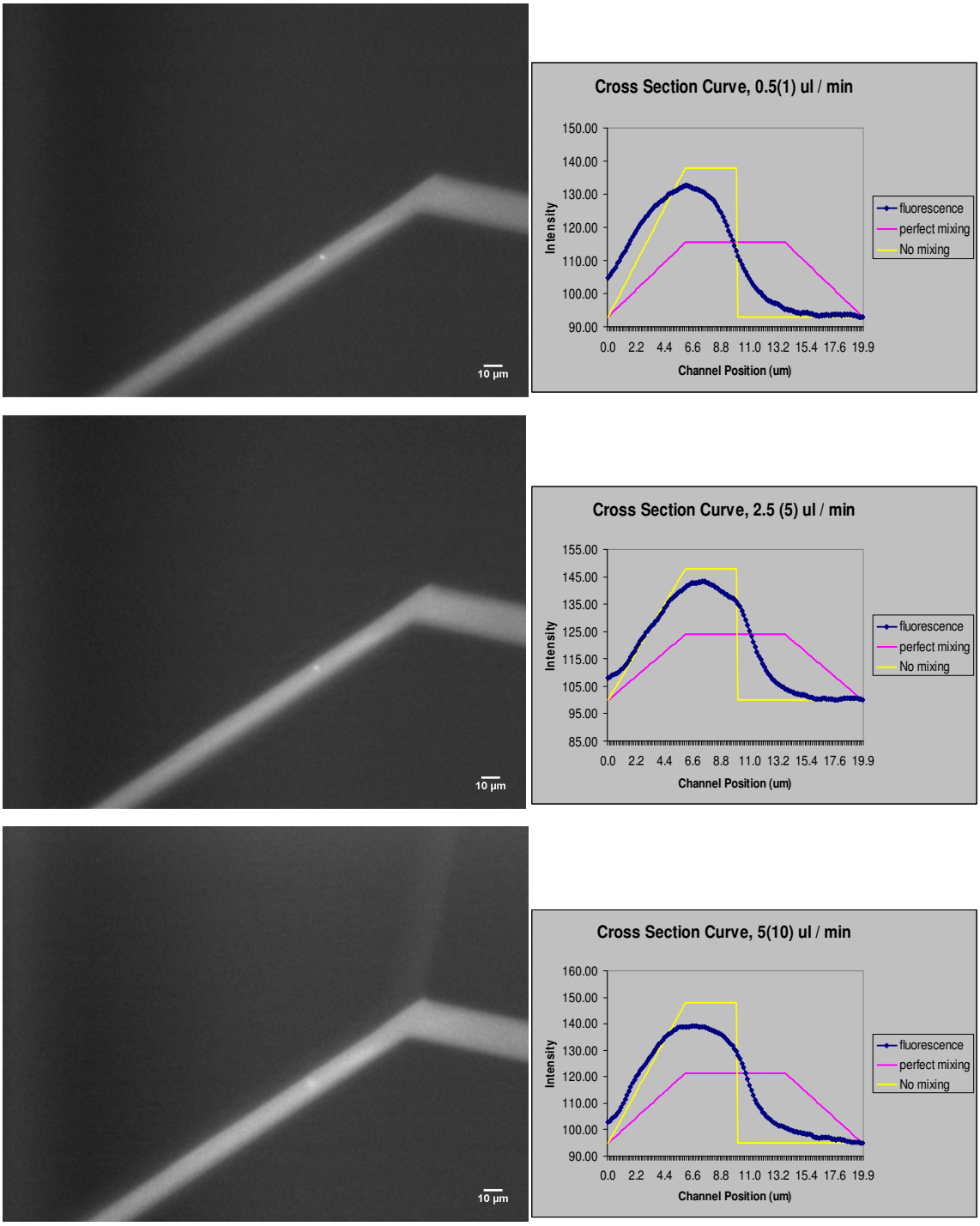

Figure 20. Y-channel at low flow rates (0.5 µL/min ~ 2.5 µL/min).

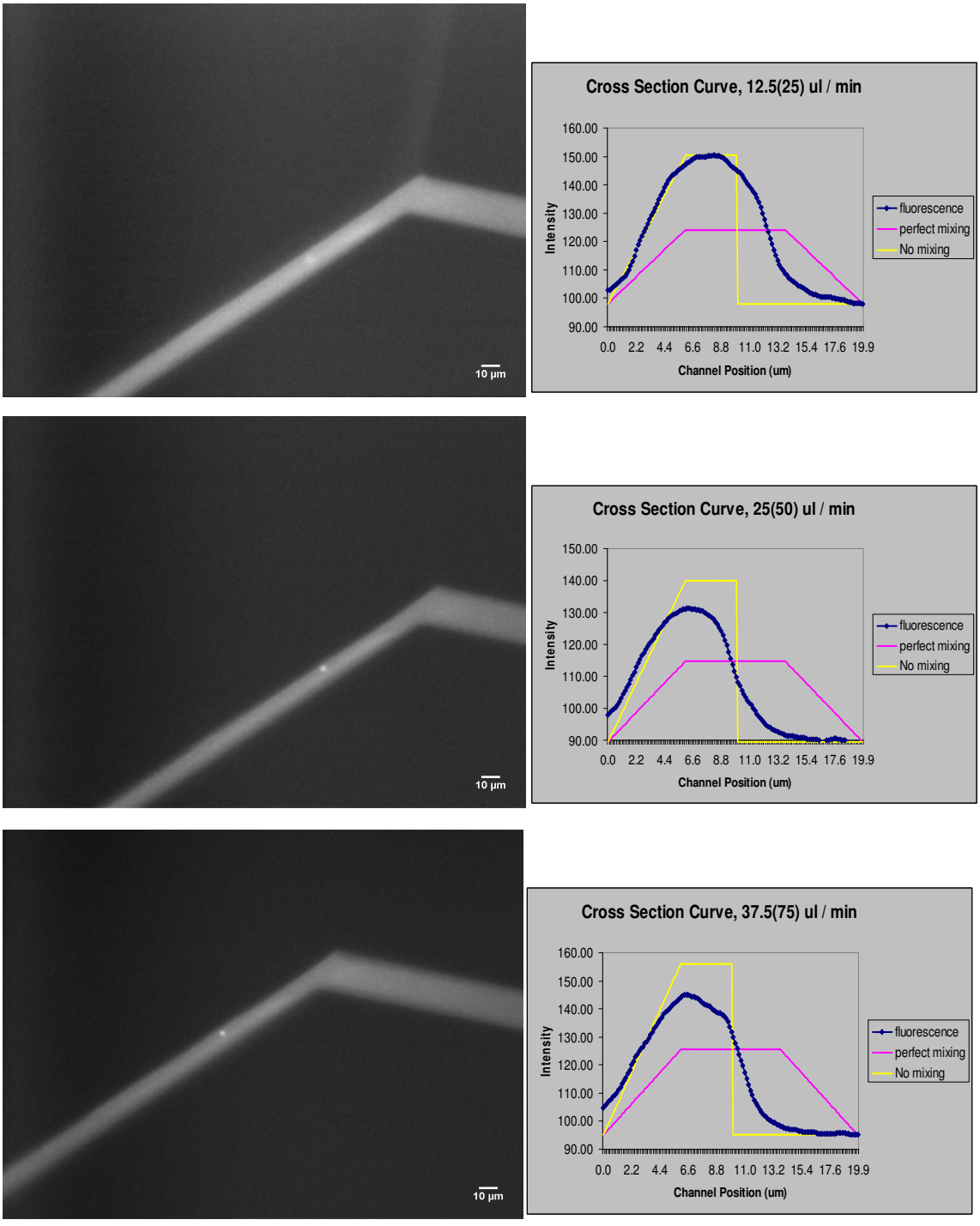

Figure 21. Y-channel at mid flow rates (12.5 µL/min ~ 37.5 µL/min).

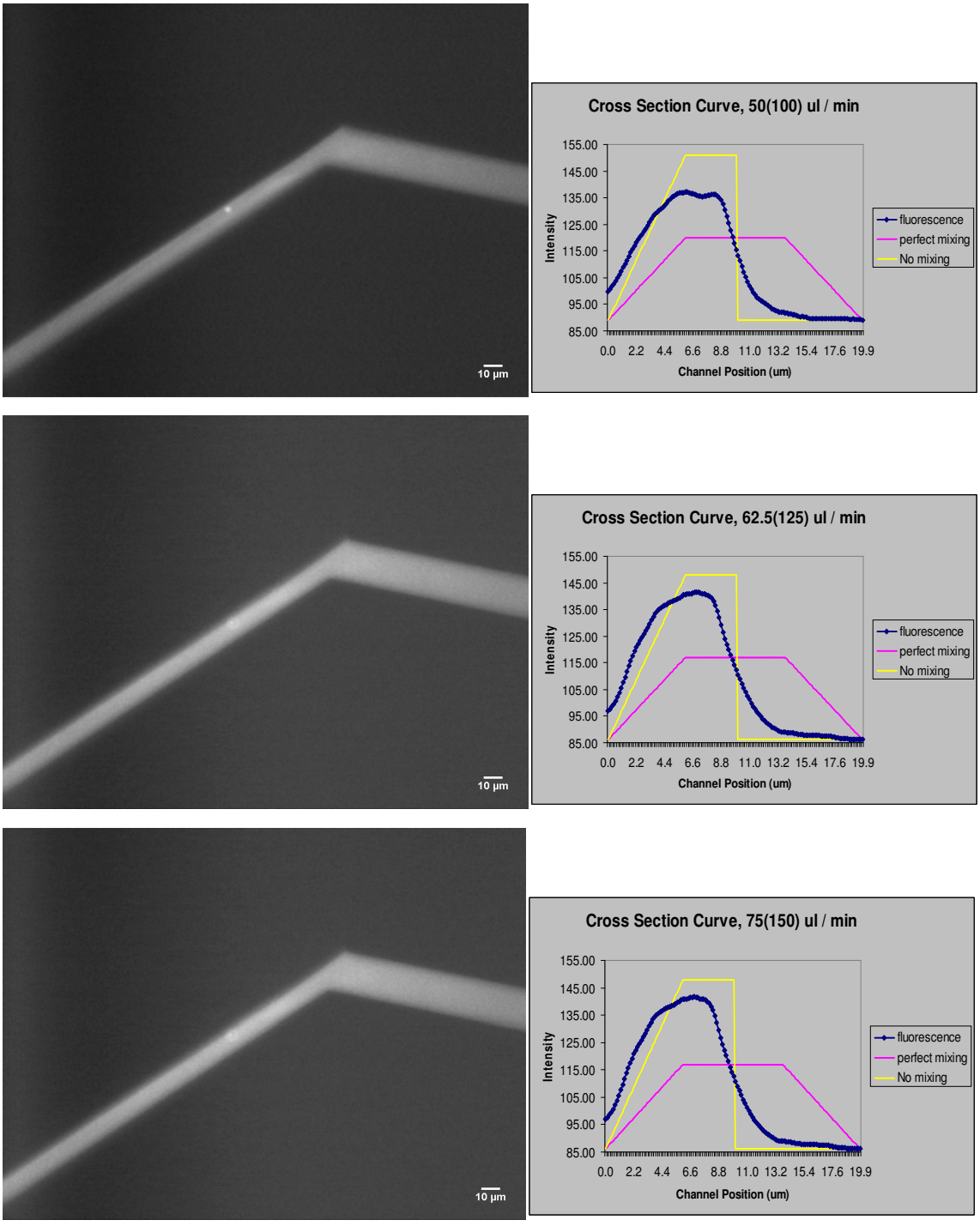

Figure 22. Y-channel at high flow rates (50 µL/min ~ 75 µL/min).

The results from the whirlpool design show promise to achieve good mixing, at around 80% at slower flow rates, and gradually dropping to 60% at 150 ul/min. Y-channel-only device showed the typical non-mixing, diffusion-only profile, and exhibit only around 20% mixing overall. The calculated R_e number ranges from 1.33 at 1 μL/min to 200 at 150 μL/min, using water viscosity = 0.001 Pa·s. Table 1 below summarizes the mixing percentage calculated, and Figure 23 shows a linearized performance chart.

Table 1. Mixing percentage for whirlpool and Y-channel at various flow rates

	Mixing Percentage (%)	
Flow Rate (μL/min)	Whirlpool	Y-channel
1	78.736	16.324
5	77.1	18.11
10	76.2	28.516
25	78.474	18.805
50	77.352	23.906
75	64.951	29.863
100	55.159	25.485
125	60.482	15.523
150	56.732	15.476
Average	69.465	21.334

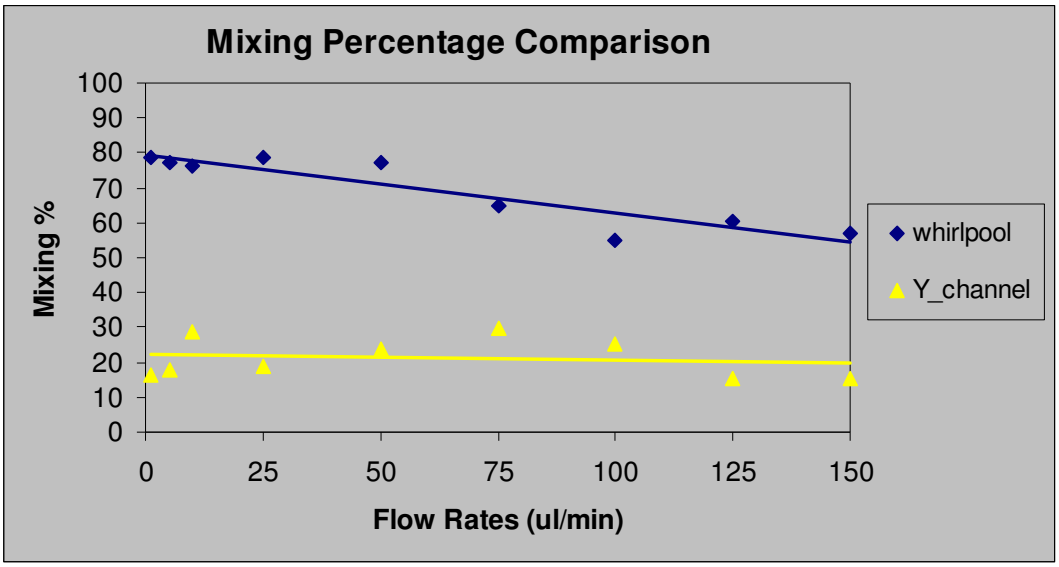

Figure 23. Overall mixing performance chart.

To provide a reference for comparison with other published designs, Table 2 below lists the performance of other passive mixers.

Table 2. Mixing performance comparison with other designs

	Mixing Length	Mixing Performance
Tesla Structure[15]	1cm for 5 pairs structure	80% @ 75 µL/min
Floored Teeth[19]	2.3 mm	70%
Self-circulation[14]	2s switching push/pull in 500 µm wide channel	75% at 8th cycle with R_e=150
Slanted wells[20]	443 µm downstream	80.5% at 8.1e^{-3} m/s

7. CONCLUSION

In this paper, we have shown that significant improvement over traditional Y-channel mixer can be achieved with a simple passive mixer design. An average of 70% mixing can be achieved within a total of 470 μm channel length, with 78.7% at 1 μL/min, compared to around 20% of the typical Y-channel. The device fabrication is simple and the device is passive thus no external power influence is required. The next step would be to incorporate several of the mixer devices in series, and achieve 100% mixing. Currently we are testing the efficiency of the Whirlpool design in series in conjunction with M.D. Anderson Cancer Center in Houston, on the effectiveness of immuno-precipitation using a micro-mixer. Immuno-precipitation is a common technique that is used to study protein interactions (see Figure 24). Two proteins, A and B for example, are to be studied of their interaction behavior. They can either be bounded to each other, or floating in solution independently with other proteins. And the goal is to separate the bounded A-B protein complex from the others. First, the antibody of A is added into the solution, along with the protein mixture and buffer solutions. A typical ratio in our experiment would consist of 30% protein mixture, 70% buffer, and about 0.5% of antibody, in a 1 c.c. sample. Then the solution is to be thoroughly mixed and allow the antibody and antigen (protein A) to bind together. Afterwards agarose gel beads are added into the solution, which seeks out the antibody and will bind with it, and become precipitation due to its bulk. After the bead volumes are washed and separated from the rest of the solution, the sample proteins will be denatured and run through electrophoresis, and be separated by their molecular weight.

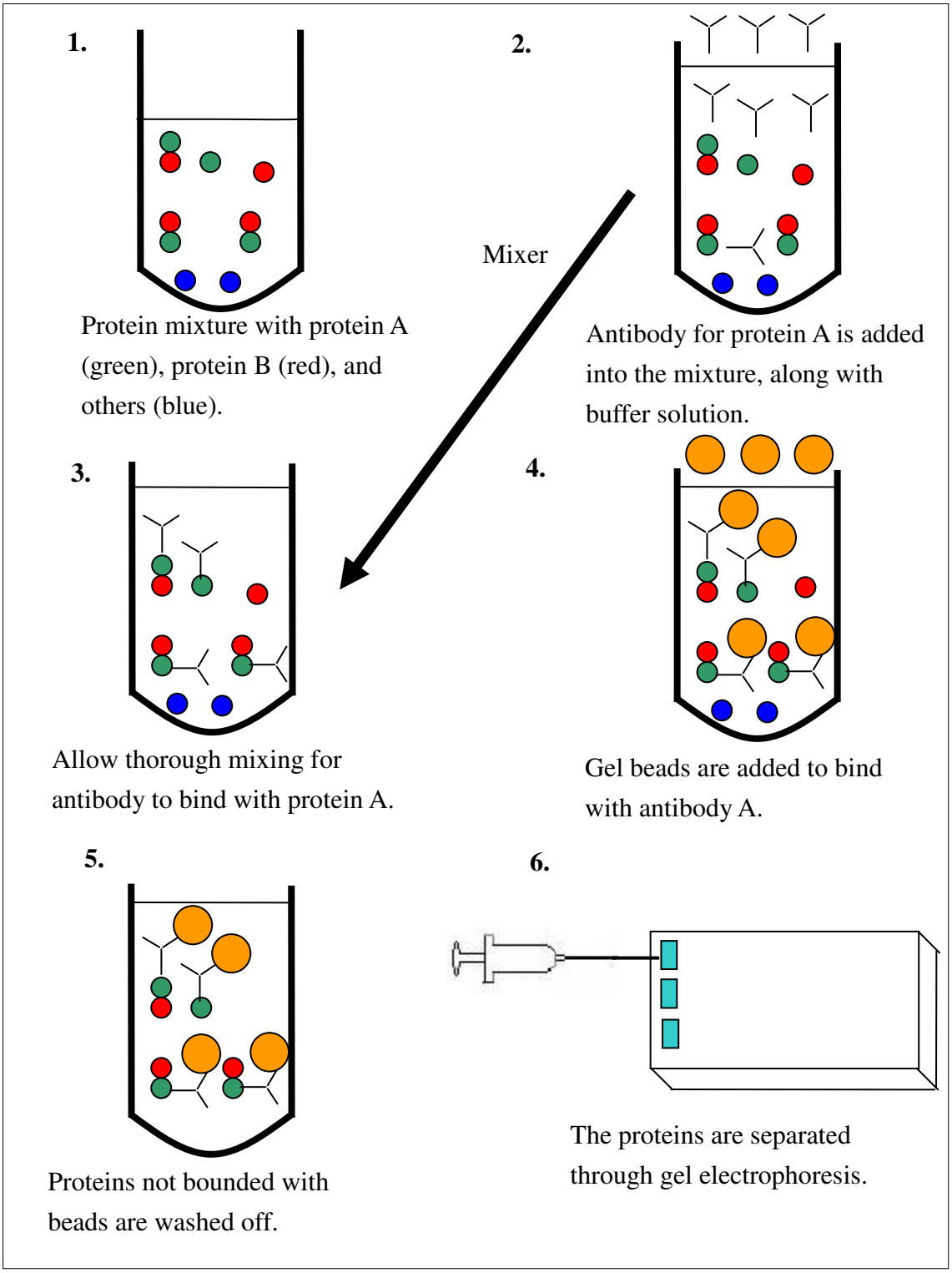

Figure 24. Immuno-precipitation procedure.

The critical step in the immuno-precipitation is to ensure proper bounding between the antibody and protein A, so that the correct ratio of protein interaction can be accounted, as inefficient mixing would cause some A-B protein complex not to bind with the antibody correctly. Traditionally the solution would be put on a mechanical shaker to mix for 24 hours at 4 ºC, mainly because of poor particle contact in bulk volume. With the micro-mixer, we are attempting to overcome this problem and to achieve the same level of mixing in 1 to 2 hours time. Current challenges include nanoport bonding to the device surface, due to increased liquid pressure from serialized mixers, and keeping an even 4 ºC temperature on the setup to ensure the survival of the protein cells. Also, devices made of both silicon-glass and PDMS (poly-dimethyl-silicane) are being tested, as in the future the devices can be manufactured from disposable PDMS materials.

REFERENCES

(1) T. Goldmann and J. S. Gonzalez, *J. Biochem. Biophys.*, 2000, **42**, 105-110

(2) Gibson B. S. Cho, T. G. Schuster, X. Zhu, D. Chang, G. D. Smith, and S. Takayama, *Anal. Chem.*, 2003, **75**, 1671-1675

(3) S. Liu, Y. Shi, W. W. Ja, and R. A. Mathies, *Anal. Chem.*, 1999, **71 (3)**, 566-573.

(4) Wagner H. Anderson and A. van den Berg, *Sens. Actuators*, 2003, **92**, 315-325.

(5) A. J. deMello, *Nature*, 2006, **442**, 394-402.

(6) J. H. Tsai and L. Lin, *Sens. Actuators*, 2002, **A 97-98**, 665-671.

(7) L. M. Fu, R.J. Yang, C. H. Lin and Y. S. Chien, *Electrophor.*, 2005, **26,** 1814-1824.

(8) G. G. Yaralioglu, I. O. Wygant, T. C. Marentis and B. T. Khuri-Yakub*, Anal. Chem.*, 2004, **76**, 3694-3698.

(9) L. H. Lu, K. S. Ryu and C. Liu, *J. Microelecmech. Syst.*, 2002, **11**, 462-469.

(10) H. Ukita and M. Kanehira, *IEEE J. Quantum Electronics*, 2002, **8**, 111-117.

(11) P. J. A. Kenis, R. F. Ismagilov and G. M. Whitesides, *Science*, 1999, **285**, 83.

(12) H. Song, M. R. Bringer, J. D. Tice, C. J. Gerdts, and R. F. Ismagilov, *Appl. Phys. Lett.*, 2003, **83**, 22.

(13) A. D. Stroock, S. K. Dertinger, A. Ajdari, I. Mezic, H. A. Stone and G. M. Whitesides, *Science*, 2002, **295**, 647-651.

(14) Y. Chung, Y. Hsu, C. Jen, M. Lu, and Y. Lin, *Lab Chip*, 2003, **4**, 70-77.

(15) C. Hong, J. Choi, and C. H. Ahn, *Lab Chip*, 2004, **4**, 109-113.

(16) T. Benzekri, C. Chandre, X. Leoncini, R. Lima and M. Vittot, *Phys. Rev. Lett.*, 2006, **96**, 124503.

(17) I. J. Sobey, in *Introduction to Interactive Boundary Layer Theory*, Oxford University Press, New York, 2000.

(18) S. H. Wong, M. C. L. Ward and C. W. Wharton, *Sens. Actuators,* 2004, **100**, 365–385.

(19) D. J. Kim, H. J. Oh, T. H. Park, J. B. Choo and S. H. Lee, *The Anal.*, 2005, **130**, 293-298.

(20) T. J. Johnson, D. Ross and L. E. Locascio, *Anal. Chem.,* 2002, **74**, 45-51.

VITA

Name:	Yao-Chung Yee
Address:	Electrical and Computer Engineering Department, Texas A&M University, 3128 TAMUS, College Station, TX 77843-3128
Email:	ycyee04@tamu.edu
Education:	B.S. Electrical and Computer Engineering, The University of Texas at Austin, 2001 M.S. Electrical and Computer Engineering, Texas A&M University, 2007